frontiers | Frontiers in Nanotechnology

TYPE Original Research
PUBLISHED 12 September 2024
DOI 10.3389/fnano.2024.1429889

OPEN ACCESS

EDITED BY
Omid Bavi,
Shiraz University of Technology, Iran

REVIEWED BY
Nestor Garcia,
CCT CONICET Córdoba, Argentina
Elham Asadian,
Shahid Beheshti University of Medical Sciences, Iran

*CORRESPONDENCE
C. Guzmán Martínez,
cguzman@uaq.mx
A. J. Rodríguez-Méndez,
jheny.rodriguez@uaq.mx

RECEIVED 08 May 2024
ACCEPTED 13 August 2024
PUBLISHED 12 September 2024

CITATION
Olvera Rodríguez I, Mora-Muñoz JM, Pérez V, Campos-Guillén J, Gallegos-Reyes MA, García-Solís P, Álvarez López A, Vallejo Becerra V, Rodríguez-Morales JA, Rodríguez-Méndez AJ and Guzmán Martínez C (2024) Development and evaluation of ibuprofen-loaded chitosan nanoparticles for pulmonary therapy.
Front. Nanotechnol. 6:1429889.
doi: 10.3389/fnano.2024.1429889

Development and evaluation of ibuprofen-loaded chitosan nanoparticles for pulmonary therapy

I. Olvera Rodríguez[1], J. M. Mora-Muñoz[1], V. Pérez[2], J. Campos-Guillén[2], M. A. Gallegos-Reyes[3], P. García-Solís[3], A. Álvarez López[1], V. Vallejo Becerra[1], J. A. Rodríguez-Morales[1], A. J. Rodríguez-Méndez[3]* and C. Guzmán Martínez[1]*

[1]Facultad de Ingeniería, División de Investigación y Posgrado, Universidad Autónoma de Querétaro, Santiago de Querétaro, Mexico, [2]Facultad de Química, División de Investigación y Posgrado, Universidad Autónoma de Querétaro, Santiago de Querétaro, Mexico, [3]Laboratorio de Neuroinmunoendocrinología, Centro de Investigación Biomédica Avanzada, Facultad de Medicina, Universidad Autónoma de Querétaro, Santiago de Querétaro, Mexico

Lung injuries are increasingly prevalent due to various diseases causing alveolar damage, potentially leading to respiratory disorders. This study employed an incubation method to develop nano-encapsulated ibuprofen within a chitosan matrix for targeted pulmonary therapy. The encapsulation was successful without altering the molecular structure of chitosan, and a 500 mg dose was identified as optimal through lung tissue cell viability and histological analysis. The controlled release mechanism of this formulation ensures targeted delivery to the lungs, reducing inflammation and promoting alveolar regeneration. This approach highlights the importance of dose optimization and presents a promising strategy to enhance the efficacy and safety of pulmonary treatments.

KEYWORDS

nanoencapsulation, alveoli, ibuprofen, chitosan, regeneration

1 Introduction

In recent years, nanotechnology has improved various scientific and industrial fields, with medical and pharmaceutical applications being particularly relevant (Mansour et al., 2023). These fields have experienced unprecedented progress due to the utilization of nanoencapsulated systems, designed to significantly optimize drug efficacy, improve solubility, enhance bioavailability, and minimize adverse side effects by encapsulating therapeutic agents (Party et al., 2023; Yang et al., 2020).

Pulmonary pathologies are prevalent worldwide due to numerous factors, such as smoking, infections, and toxins, leading to chronic or acute diseases. These conditions, though generally treatable, can become fatal or cause a permanent reduction in lung function if alveolar damage occurs (McGee et al., 2020; Patrisio, 2020). The COVID-19 pandemic, from 2020 to 2022, exacerbated this issue, causing widespread cases of pneumonia and resulting in thousands of deaths due to alveolar damage (Ambasch et al., 2021).

The alveoli play a fundamental role in the respiratory system, being responsible for gas exchange. Consequently, damage to these structures directly impairs lung function and causes significant pain and discomfort (Pontes and Grenha, 2020). Despite the availability

of numerous therapeutic agents, their side effects, necessary higher doses, and systemic risks often counteract their benefits (He et al., 2022; Newman, 2017). This problem necessitates innovative drug delivery methods explicitly targeting the lungs, offering relief while mitigating systemic risks.

Ibuprofen, a nonsteroidal anti-inflammatory drug (NSAID), has historically been one of the most widely used medications for managing inflammation (Ha and Paek, 2021; Party et al., 2023). Although its widespread use undeniably shows therapeutic benefits, prolonged or improper use can lead to numerous health complications, such as stomach ulcers, kidney damage, and cardiovascular problems (Xu et al., 2023). However, it is appropriate and targeted administration through nanoencapsulation holds promise for treating pulmonary inflammations due to its anti-inflammatory effects (Baek et al., 2017).

Chitosan is a biocompatible and biodegradable material with notable anti-inflammatory and regenerative properties (Gulati et al., 2021). Its applications in wound healing have been reported over the years, highlighting its potential to promote tissue regeneration (Liu et al., 2018). Additionally, chitosan has been used in the controlled release of drugs when employed as a matrix in nanoencapsulated compounds (Chatterjee and Hui, 2019; Huang et al., 2017).

Nanoencapsulation of ibuprofen in a chitosan matrix offers a dual benefit. First, it utilizes the anti-inflammatory properties of ibuprofen to control pain (Gliszczyńska and Sánchez-López, 2021) Simultaneously, the regenerative properties of chitosan promote alveolar healing and regeneration (Kim et al., 2023). Furthermore, this encapsulation nanosystem enables controlled drug release to the alveolar region, potentially reducing the systemic side effects associated with traditional drug administration.

In this study, we have developed a multifunctional nanocomposite of ibuprofen encapsulated in a chitosan matrix, combining the therapeutic properties of ibuprofen with the regenerative capacities of chitosan to repair damaged alveoli. We have analyzed the methodologies employed, described the results from studies in rodents, and discussed the implications of our findings in pulmonary medicine.

To address the critical issue of dose-dependent efficacy and safety, we have evaluated the effects of ibuprofen at doses of 1,000 mg, 500 mg, and 250 mg. These specific dosages were selected based on their relevance to achieving a therapeutic balance between efficacy and minimizing adverse effects. Higher doses (1,000 mg) are investigated to understand the upper limit of anti-inflammatory benefits, whereas moderate (500 mg) and lower doses (250 mg) are explored for their potential to provide sufficient therapeutic outcomes while reducing the risk of systemic side effects. This range of dosages allows for a comprehensive assessment of the optimal therapeutic window for treating pulmonary inflammation with ibuprofen-loaded chitosan nanoparticles.

2 Materials and methods

2.1 Reagents

The reagents used for the experimentation were low molecular weight chitosan (Sigma-Aldrich CAT: 448869-250G), sodium tripolyphosphate (TPP) (Sigma-Aldrich CAT:238503-500G), 99.7% glacial acetic acid (J. T. Baker CAT: 9508-05), 28.0%–30.0% ammonium hydroxide (J. T. Baker CAT: 9721-03) and 37% hydrochloric acid (J. T. Baker CAT: 4218-03), which were used without additional purification; In addition, tridistilled water (Technology and control) and ethanol absolute (Biopack) were used. The active ingredients were ibuprofen (Sigma Aldrich).

2.2 Synthesis of chitosan matrix

For the synthesis of chitosan nanoparticles (chitosan NPs), the ionic gelation method was chosen based on the report by Calvo et al. (1997), with certain parameter modifications according to Hassani et al. (2015). This method uses a cross-linking agent, in this case, TPP, in different concentrations, which was slowly added dropwise into chitosan solutions, which was slowly added dropwise into chitosan solutions. These solutions were previously prepared using a 1% acetic acid solution (v/v) and magnetic stirring for about 2 h. The dripping was carried out with the help of a peristaltic pump, and the flow rates were around 0.1 mL/min, all while the solution in question was vigorously stirred at 750 rpm. Once the dripping had finished, the samples were left to react for 60 min and vortexed for 5 min. Once the samples were ready, they were placed in an ultrasonic bath for short periods (5–10 min) at room temperature to achieve good dispersion and reduce the size.

2.3 Ibuprofen encapsulation process

To introduce the active ingredient, the incubation method was used. Chitosan NPs were prepared in solution and subsequently mixed with ibuprofen solutions at a specific concentration of 2 mg/mL. The ibuprofen solution was added to the chitosan NPs solution using a peristaltic pump to ensure controlled and consistent addition. The mixtures were then stirred vigorously for 60 min to ensure thorough adsorption of ibuprofen onto the surface of the chitosan NPs (Gan & Wang, 2007). In this method, the active ingredients are anchored to the chitosan NPs solely by surface adsorption.

2.4 Scanning electron microscopy (SEM) analysis

The scanning electron microscopy (SEM) technique was used with a JEOL JSM-7610F microscope to identify the morphology of the obtained particles and verify their size and distribution.

2.5 Dynamic light scattering (DLS) analysis

To characterize the NPs, particle size analysis was performed using a dynamic light scattering instrument (Malvern Instruments Zetasizer Nano).

2.6 Encapsulation efficiency analysis

The NPs were precipitated with the loaded drug (using a basic NH_4OH solution and centrifugation), and the supernatant

medium was taken as a sample to determine the loading efficiency. Subsequently, the amount of free drug in the solution (unloaded drug) was determined by UV-Vis spectroscopy (using Beer-Lambert law and a calibration curve constructed from solutions of known concentration at 195 and 218 nm). The efficiency of the drug encapsulated in the NPs was calculated using the formula reported by Saha et al. (2010) (Equation 1), where the amount of drug used is related to the amount of free drug in the solution.

$$Encapsulation\ Efficiency = \frac{\left(T_p - T_F\right)}{T_p} * 100 \quad (1)$$

Where T_p is the initial amount of drug used for loading into the nanoparticles, T_F is the amount of drug measured in the supernatant (unloaded drug).

2.7 Fourier transform infrared spectroscopy (FTIR) analysis

Fourier transform infrared spectroscopy (FTIR) was performed using a PerkinElmer FT-IR Spectrum Two instrument to determine the interactions between the components, including both the bare NPs and the drug-loaded NPs, to analyze their interactions within the structure.

2.8 *In vitro* analysis (MTT assay)

The impact of Chitosan NPs and Chitosan-Ibuprofen-loaded NPs on A549 cell viability was assessed using the MTT assay (CyQUANT MTT Cell Proliferation Assay Kit Protocol, 2024). A549 cells were seeded at a density of 7.5×10^3 cells per well in a 96-well plate and allowed to stabilize for 48 h. Following stabilization, cells were treated in triplicate with Chitosan-IB NPs (1,000 mg, 500 mg, 250 mg) or Chitosan NPs unloaded. After 24 h of treatment, cells were washed with PBS, and MTT solution (0.5 mg/mL) was added for 4 h to induce formazan crystal formation. Dimethyl sulfoxide (DMSO) was then used to dissolve the crystals, and absorbance was measured at 550 nm using a Thermo Scientifi™ Multiskan™ GO Microplate Spectrophotometer (Fisher Scientific). Cell viability was calculated according with Equation 2:

$$Relative\ cell\ vioability = \frac{control\ ABS_{550} - sample\ ABS_{550}}{control\ ABS_{550}} * 100 \quad (2)$$

Where control ABS_{550} is the absorbance value of the control plate, sample ABS_{550} is the absorbance value of each sample according with the well.

2.9 *In vivo* analysis

To validate the therapeutic potential of the ibuprofen-loaded chitosan nanoparticles observed *in vitro*, we conducted *in vivo* experiments in a rat model of acute lung injury. Female Sprague-Dawley (SD) rats, weighing between 220 and 250 g at approximately 6 weeks of age, were housed in the avian facilities of the UNAM bioterium in Juriquilla, Qro, under a 14 L:10D photoperiod with *ad libitum* access to commercial food and water.

Acute lung injury was induced by intravenous administration of oleic acid (OA). Briefly, OA was diluted in 70% ethanol and physiological saline to a concentration of 25 mg/mL, and the pH was adjusted to 7.5. Rats were anesthetized with an intravenous dose of ketamine (15 mg/kg) via the jugular vein, and OA was subsequently administered at a rate of 20 mg/kg/min for 5 min via the same route. In 250 g rats, this equated to a 1 mL dose of the OA solution.

We hypothesized that the nanoparticles would mitigate inflammation and promote alveolar repair *in vivo*. To assess this, nanoparticle treatment (1 mL) was administered intravenously 30 min and 24 h after OA injury. Blood samples were collected at 0-, 1-, 24-, and 48-h post-injury to evaluate potential alterations in lung function (e.g., hemoglobin levels). Rats were sacrificed at 48 h, and lung tissue was collected for histological analysis to assess the extent of alveolar damage and repair.

All procedures were conducted in compliance with the guidelines approved by the Committee on Bioethics CEAIFI-151–2021-PI.

2.10 Plasma free hemoglobin test

Hemoglobin levels in rat blood were determined spectrophotometrically at 415, 450, and 700 nm according to Fairbanks et al. (1992), with calibration following the method of ROSA et al. (2020). Higher hemoglobin levels were indicative of improved pulmonary condition (Auvinen et al., 2021).

2.11 Histopathological evaluation

The tissues (lung, liver) were collected and were fixed in PFA 10% for 24–48 h at room temperature, dehydrated in ethanol, and embedded in paraffin wax. Tissue sections (7 μm thick) were then cut using a microtome and mounted onto charged glass slides (Superfrost/Plus, Fisher, Pittsburgh, PA).

Histopathologic examination was also performed to determine signs of cellular infiltration and edema in the lung tissue using hematoxylin–eosin staining. All tissues were examined by histopathologist in a double-blind analysis, and presence of alterations were classified by percentage of the area affected (Türkmen et al., 2024).

Serial tissue sections were cleared in xylol [Baker], 3 times (3x) during 5 min, rehydrated in a graded series of ethanol (absolute, 2 × 5 min; 96% 2 × 5 min; 70%, 5 min; 50%, 5 min; deionized water 5 min), and equilibrated in water (1 min). Slides were incubated with Harris hematoxylin (0.5% hematoxylin [Merck, Darmstadt, Germany] in 5% absolute ethanol, 10% aluminum potassium sulfate [Sigma, St. Louis, MO], 0.25% mercury (II) oxide red [Aldrich, St. Louis, MO] for 3 min, rinsed with water with agitation for 1 min and rapidly passed through acidic alcohol (0.1% HCl in 70% alcohol), washed in water for 1 min and then dipped five times in ammoniacal water (0.1% NH_4OH in deionized

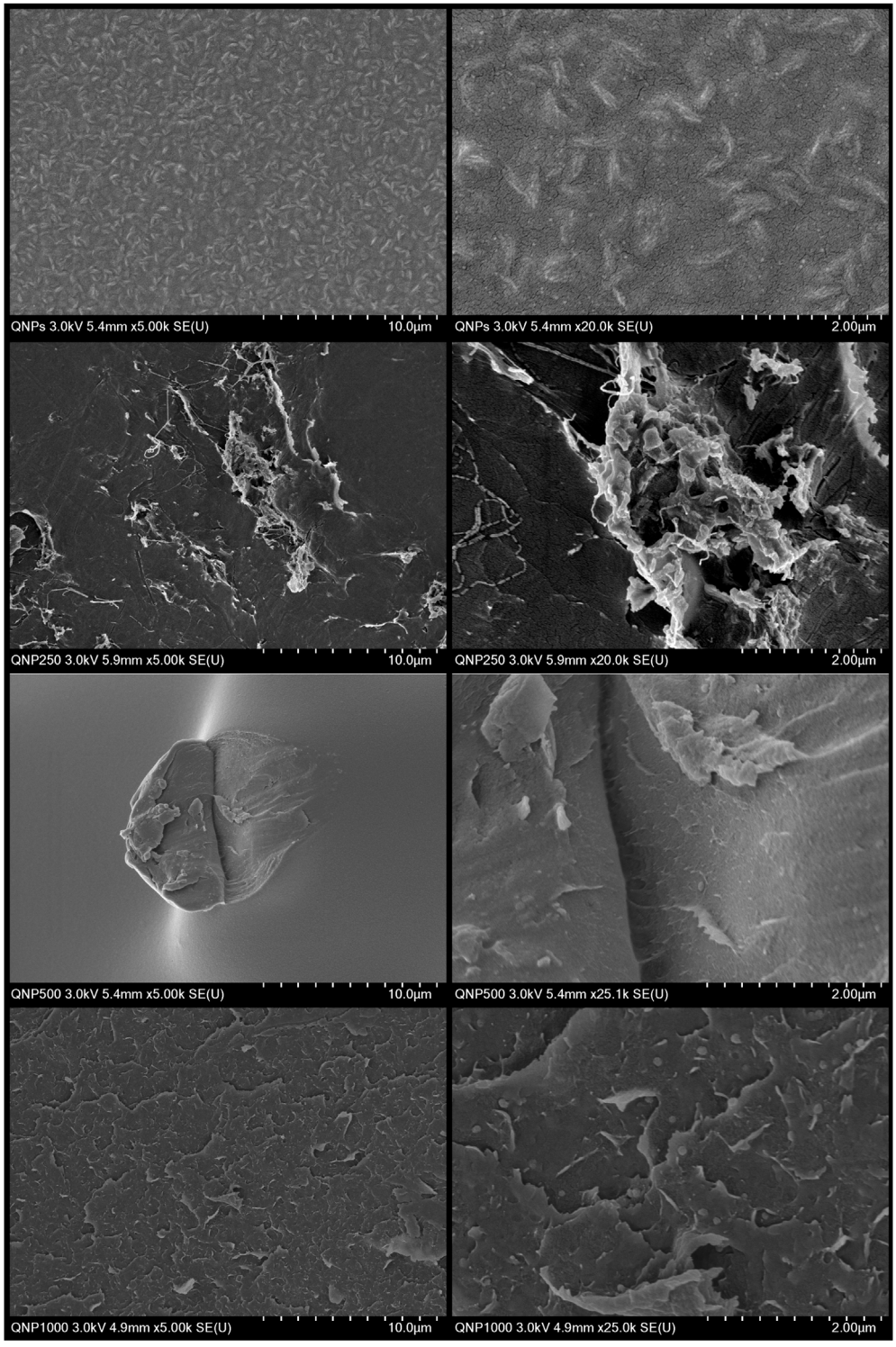

FIGURE 1
SEM images of chitosan nanoparticles (Np) and chitosan-IB Np films. **(A)** Chitosan Np at ×5,000 magnification. **(B)** Chitosan Np at ×20,000 magnification. **(C)** Chitosan-IB (250 mg) Np at ×1,000 magnification. **(D)** Chitosan-IB (250 mg) Np at ×2,500 magnification. **(E)** Chitosan-IB (500 mg) Np at ×1,000 magnification. **(F)** Chitosan-IB (500 mg) Np at ×10,000 magnification. **(G)** Chitosan-IB (1,000 mg) Np at ×2,500 magnification. **(H)** Chitosan-IB (1,000 mg) Np at ×4,900 magnification.

water) and rinsed in distilled water for 1 min. The slides were then incubated in eosin Y [Sigma], 0.25% in 60% acidified alcohol) for 15 s, rinsed with water and then dehydrated in a graded series of ethanol (70%, 96% 3x, 100%3). All sections were then dipped in two baths of xylol (3x each) before mounting permanently using Entellan [Merck].

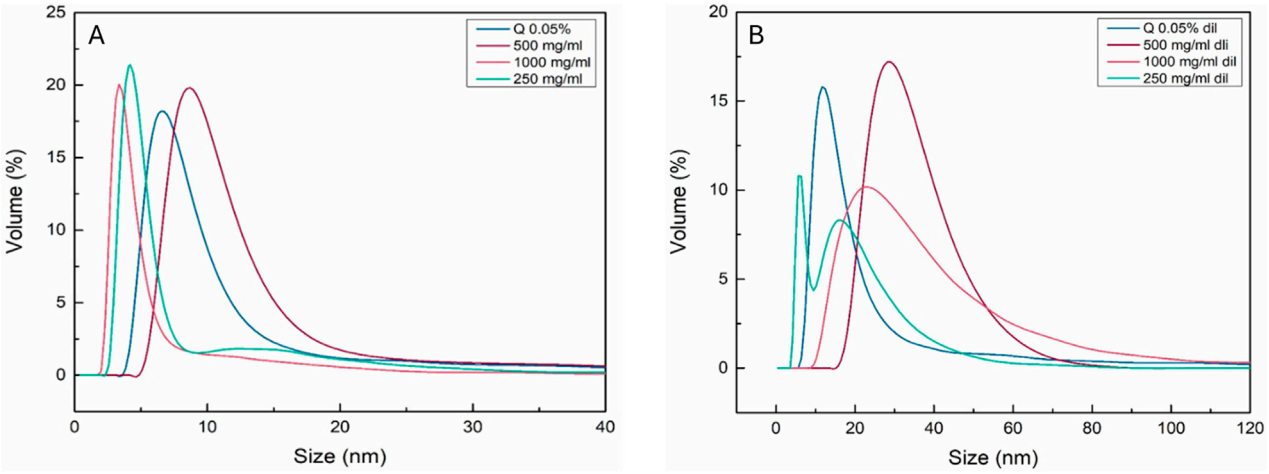

FIGURE 2
DLS analysis of chitosan nanoparticles (Np) and chitosan-IB Np systems. **(A)** Hydrodynamic diameter distribution of Chitosan Np, Chitosan-IB (1,000 mg) Np, Chitosan-IB (500 mg) Np, and Chitosan-IB (250 mg) Np at high concentration. **(B)** Hydrodynamic diameter distribution of the same systems diluted 10-fold.

3 Results

3.1 Scanning electron microscope (SEM) analysis for chitosan Np and Chitosan-IB np

To prepare samples for scanning electron microscopy (SEM) analysis, Chitosan Np and Chitosan-IB Np were dispersed onto a thin chitosan film and subsequently sputter-coated with a thin layer of gold. Figure 1A depicts the SEM image of Chitosan Np, revealing surface irregularities attributed to the presence of the nanoparticles. A higher magnification image (Figure 1B) further illustrates these irregularities as elongated structures. This morphology may be a result of the nanoparticle fixation process onto the chitosan film, potentially causing aggregation or alignment during drying.

The SEM image in Figure 1C, representing films with Chitosan-IB (250 mg) Np, reveals significant agglomeration of material on the surface, with numerous zones exhibiting high nanoparticle density. Upon closer inspection in Figure 1D (a zoomed-in view), the agglomerated material appears to alter the morphology of individual particles, resulting in a thread-like appearance. This morphological change suggests that the agglomeration process may induce particle-particle interactions that lead to the formation of elongated structures.

In contrast to previous images, the SEM image of the film with Chitosan-IB (500 mg) Np (Figure 1E) appears to have a lower particle density. However, upon closer inspection of the central region, certain structures suggest the presence of nanoparticles. A zoomed-in view of this area (Figure 1F), particularly within a scratch on the film, reveals distinct and well-defined particles. Despite the seemingly low nanoparticle density, this observation confirms their presence and demonstrates that even at lower concentrations, the nanoparticles can be visualized and identified through SEM analysis.

Finally, in the film loaded with Chitosan-IB (1000 mg) Np, irregularities are observed at the film's edge (Figure 1G), likely due to the presence of nanoparticles. Zooming in on this edge region (Figure 1H), the nanoparticles become more visible, exhibiting a consistent size and shape within the observed field. This consistency suggests a uniform distribution of nanoparticles at higher concentrations, potentially forming a more continuous layer on the film surface.

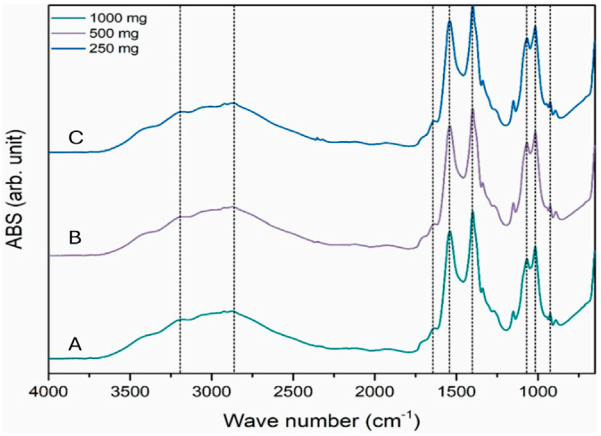

FIGURE 3
FTIR spectra of chitosan-IB nanoparticles at different drug loadings: **(A)** 1,000 mg, **(B)** 500 mg, and **(C)** 250 mg.

3.2 Dynamic light scattering (DLS) analysis or chitosan unloaded and loaded

The particle size was measured in two cases. In the first case, shown in Figure 2A, the concentration of the nanoparticle system was high. When the system contained only chitosan, the size was about 6 nm. When loaded with 250 mg/mL of ibuprofen, the size decreased to 3.5 nm. With 500 mg/mL of ibuprofen, the size increased to 9 nm, and with 1,000 mg/mL, the size was 3 nm. The size distribution shows no discernible trend in the system as a

function of ibuprofen loading. This effect is likely due to the interaction between the polymer chains and the molecule of the drug or to the fact that the concentration promotes the interaction of the electrical charges in the solution as can be seen in the SEM images, which causes compression in the chitosan matrix.

In the second stage in Figure 2B, the solution of the nanoencapsulated system was diluted to maintain the size of the chitosan particles. The tendency in the size when the system was loaded is present. The size of the system when the ibuprofen was 250 mg/mL was bimodal and had a size of 1 nm and 15 nm, then the system loaded with 500 mg/mL reached 30 nm. When 1,000 mg/mL was present in the system, the size was 22 nm; the increase in size is due to the agglomeration of the particles to maintain the stability of the suspension.

3.3 Fourier transform infrared spectroscopy (FTIR) analysis

The FTIR spectra in Figure 3 corresponding to the nanocapsulated system of chitosan-ibuprofen generally show no significant shift in intensity and signals depending on the different content of ibuprofen in the chitosan matrix in all cases, indicating that the ibuprofen is wholly contained in the chitosan matrix and does not cause any changes or modifications in the molecular structure of the chitosan polymer, implying that the nanocapsulated system was successful.

Moreover, the characteristic IR signals of chitosan are present in the spectra; the signals corresponding to - OH stretching are at 3,240 cm^{-1}, at 2,800 cm^{-1}, the NH_2 stretching signal is present, the amide I and II are at 1,680 cm^{-1} and 1,400 cm^{-1}, respectively, and the signal in the range between 900 cm^{-1} and 1,100 cm^{-1} is the C-O-C stretching signal, which remained unchanged after encapsulation.

The lack of a clear trend in particle size with varying ibuprofen loading, as measured by DLS, suggests that chitosan's ability to encapsulate ibuprofen and adjust its size is responsible for the observed patterns. This conclusion is supported by FTIR spectroscopy, which shows characteristic chitosan signals without significant shifts or changes in intensity, indicating that ibuprofen loading does not alter the fundamental chemical structure of chitosan.

3.4 Encapsulation efficiency analysis

The incubation method demonstrated high encapsulation efficiency for all tested drug concentrations (1,000 mg, 500 mg, and 250 mg). In all cases, the encapsulation efficiency exceeded 80%, indicating that most of the drug was successfully incorporated into the nanoparticles during this process. This result highlights the effectiveness of incubation as a reliable and efficient method for drug encapsulation in the present study.

3.5 *In vitro* analysis

The observed viability of cells in the various dilutions of chitosan nanoparticles shows a moderately decreasing trend as the dilution becomes more severe, according to the presence of chitosan observed in Figure 4A. Remarkably, the variation in viability between dilutions remains minimal, with a maximum difference of only 3% between the densest and the most dilute concentrations. This result suggests that the A549 cells exhibit a relatively uniform level of viability when exposed to different concentrations of chitosan nanoparticles. The results could indicate the biocompatibility of chitosan nanoparticles with the A549 cell line or a limited cytotoxic effect within the concentration range tested.

Additionally, the results indicate a dose-dependent decrease in A549 cell viability with increasing concentrations of ibuprofen delivered via chitosan nanoparticles. In Figure 4B, the initial minimal effect at 15.625 mg suggests a higher tolerance of cells at lower doses of ibuprofen. However, as the concentration increases, the more pronounced cytotoxic effects become apparent, with a marked decrease in cell viability from 97% to 70% throughout the range of ibuprofen tested. This highlights the potential impact of drug volume on cellular responses and underscores the importance of careful dosing when using chitosan nanoparticles as drug carriers.

The extended range of ibuprofen concentrations emphasizes the dose-dependent decrease in A549 cell viability. While the decrease from 150 mg (95% viability) to 200 mg (83% viability) is quite pronounced in Figure 4C, subsequent increases in ibuprofen loading lead to a more gradual decrease in cell viability. This could indicate a certain saturation or tolerance threshold of the cells, beyond which they react less dramatically to increased drug concentrations. Remarkably, the cells retained 70% viability even at the highest dose of 500 mg, indicating a possible resistance of the A549 cell line to ibuprofen when administered via chitosan nanoparticles.

The highest concentrations of ibuprofen in Figure 4D showed an intriguing pattern of A549 cell viability. The slight increase from 70% (500 mg) to 75% (600 mg) suggests nonlinear responses or possible experimental fluctuations at these high drug concentrations. The subsequent decreases and fluctuations at 900 mg illustrate the complexity of cellular responses at such high concentrations of ibuprofen. The data illustrates that although there is a general trend towards decreased viability at high ibuprofen concentrations, the relationship is not strictly linear, especially at very high concentrations. This highlights the complexity of drug-cell interactions and the need for thorough pharmacodynamic and pharmacokinetic studies when considering drug delivery via nanoparticles.

3.6 Hemoglobin analysis

In Figure 5 presents the free hemoglobin levels in rats over a 48-h period. Control rats maintained a stable hemoglobin range of 15.0–15.5 mg/dL. In contrast, oleic acid-injured rats initially experienced a decrease in hemoglobin (11.4–14.7 mg/dL), but levels increased to 15.0–16.4 mg/dL within 1 hour of receiving either Chitosan NP or Chitosan-IB NP.

At 24 h, the 250 mg/mL and 1,000 mg/mL nanoparticle doses resulted in decreased hemoglobin levels (13.9 and 14.7 mg/dL, respectively). However, following a second dose at 48 h, both groups showed an increase, reaching levels comparable to the control group (14.7 and 14.9 mg/dL). Notably, the 500 mg/mL

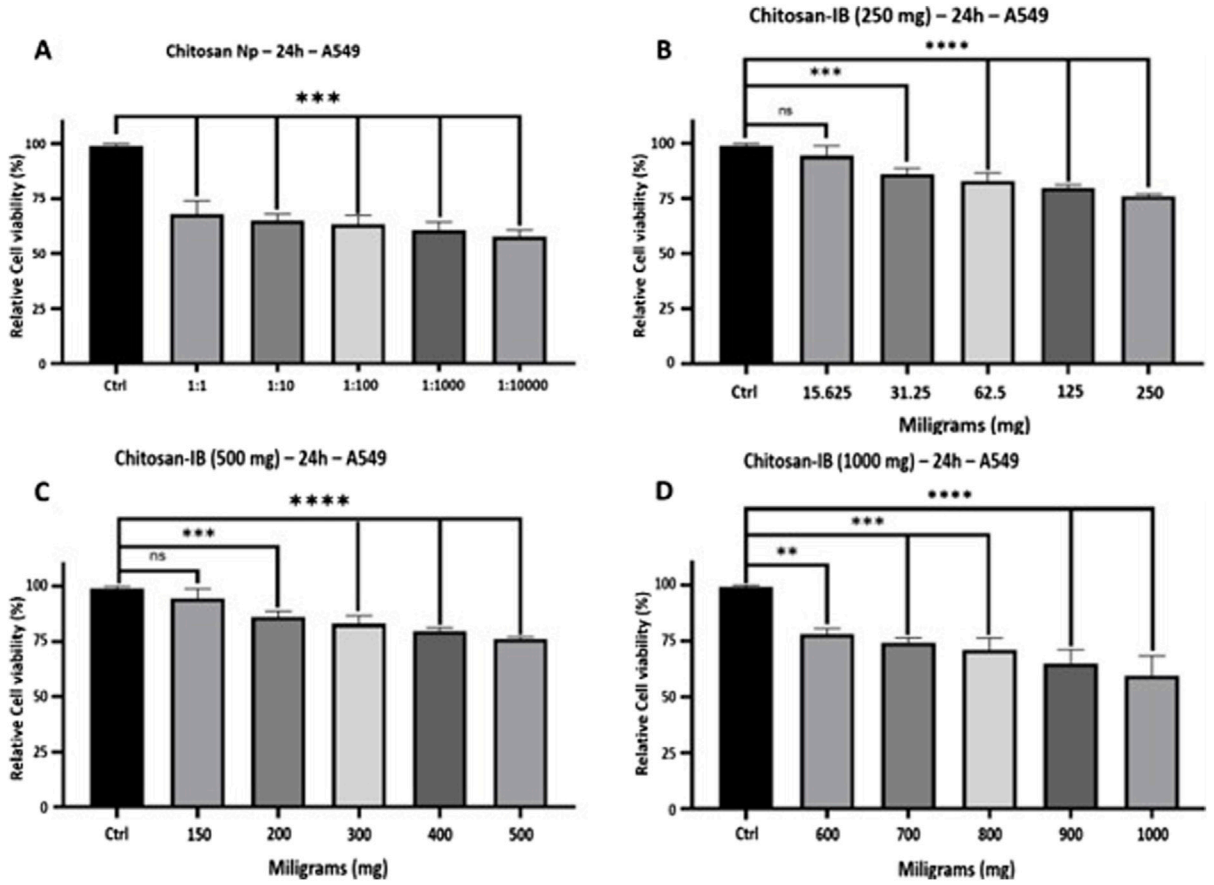

FIGURE 4
In vitro cell viability analysis of chitosan-based nanoparticles using MTT assay. **(A)** Chitosan Np. **(B)** Chitosan-IB (250 mg) Np. **(C)** Chitosan-IB (500 mg) Np. **(D)** Chitosan-IB (1,000 mg) Np.

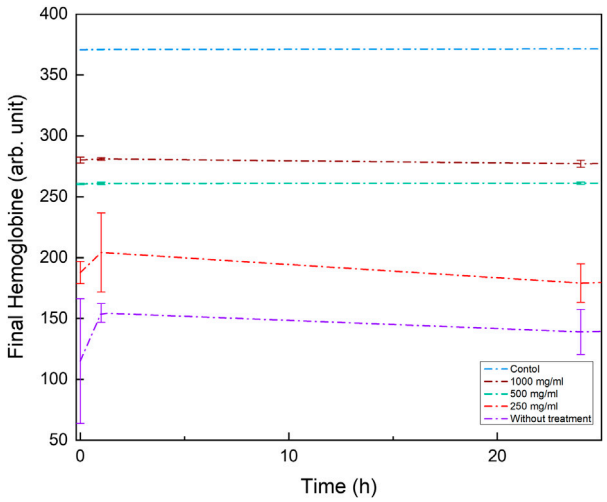

FIGURE 5
Hemoglobin levels in rats after treatment with chitosan-based nanoparticles. The graph shows the comparison of hemoglobin levels in rats treated with Chitosan Np, Chitosan-IB (1,000 mg) Np, Chitosan-IB (500 mg) Np, and Chitosan-IB (250 mg) Np, assessed to determine the potential impact of treatments on the health of the animals.

dose maintained a consistent hemoglobin level of 15.1 mg/dL at 24 h.

3.6.1 Initial increase

The initial increase in hemoglobin could be a compensatory mechanism triggered by lung injury and inflammation of the alveolar epithelium. This inflammation might impair oxygen exchange in the lungs, leading the body to produce more hemoglobin to try and enhance oxygen transport.

3.6.2 Subsequent decrease

The decrease in hemoglobin after 24 h may indicate depletion of the epithelial tissue due to the ongoing injury. As the epithelial cells are damaged, they are less able to produce hemoglobin, leading to a decline in its levels.

3.6.3 Higher doses

The fact that higher doses of the Chitosan-IB Np (500 and 1,000 mg/mL) did not cause the same fluctuations in hemoglobin levels as lower doses suggests a different mechanism of action or a threshold effect. This indicates that these higher doses might be less toxic and potentially fall within a therapeutic window. Therefore, they are promising candidates for *in vivo* testing, although further research is needed to confirm their safety and efficacy. This research

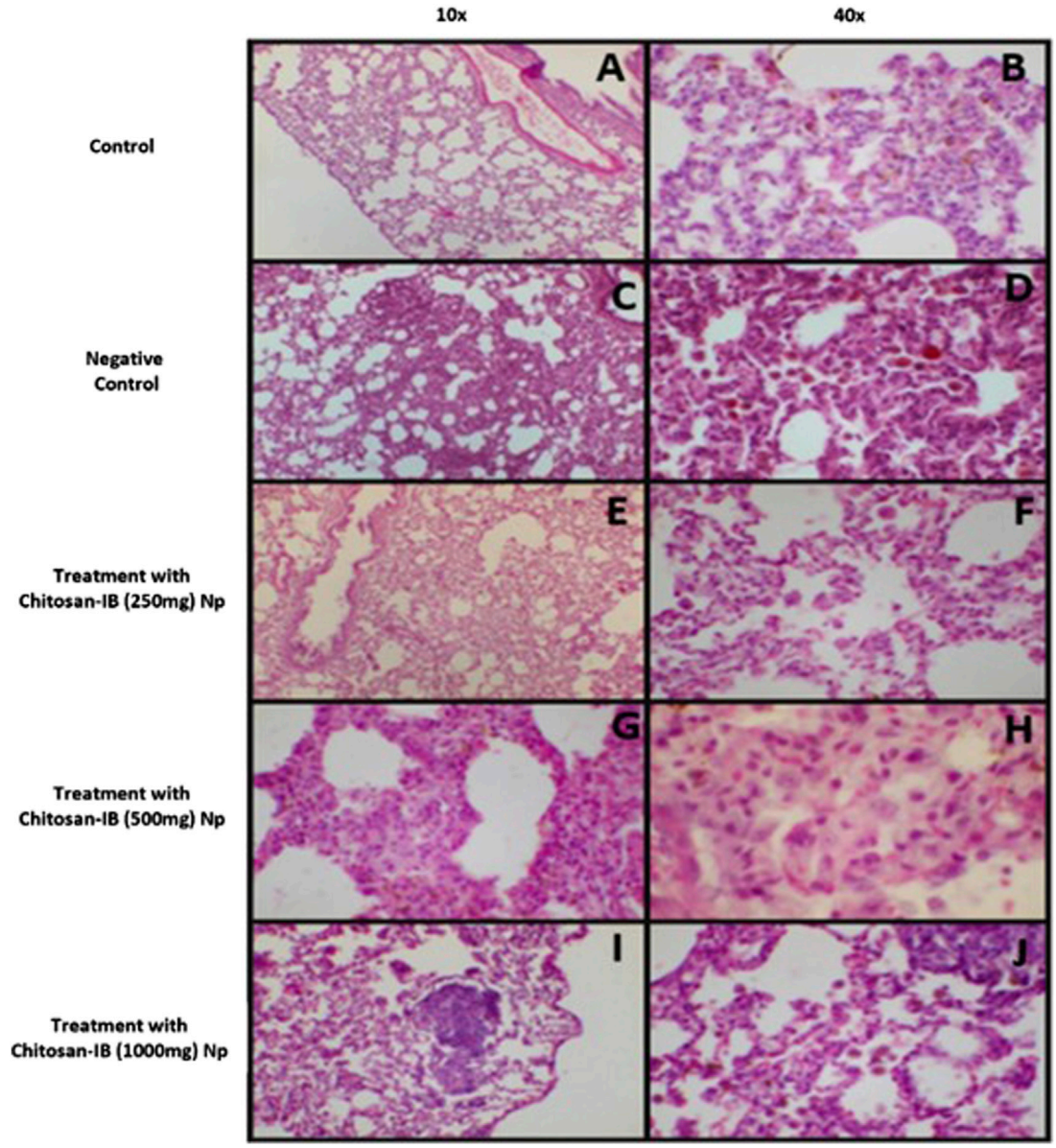

FIGURE 6
Histological analysis of rat lung tissue (H&E stain); **(A,B)**: Healthy lung tissue from control rats [**(A)**: 10X, **(B)** 40X]; **(C,D)**: Lung tissue from negative control rats [**(C)**: 10X, **(D)** 40X]; **(E,F)**: Lung tissue from rats treated with Chitosan-IB (250 mg) Np [**(E)**: 10X, **(F)**: 40X]; **(G,H)**: Lung tissue from rats treated with Chitosan-IB (500 mg) Np [**(G)**: 10X, **(H)**: 40X]; **(I,J)**: Lung tissue from rats treated with Chitosan-IB (1,000 mg) Np [**(I)**: 10X, **(J)** 40X].

would involve additional *in vitro* and *in vivo* studies to assess both short-term and long-term effects and to determine the optimal dose that balances efficacy with safety.

The observed increase in hemoglobin in untreated and lower-dose nanoparticle groups, followed by a subsequent decrease, indicates a complex physiological response. The stable hemoglobin level maintained by the 500 mg/mL dose suggests that it may be a more optimal treatment option. Although the 1,000 mg/mL dose exhibited a similar hemoglobin curve, the *in vitro* results indicate that it does not offer additional benefits compared to the 500 mg/mL dose.

The references to (Gaggar and Patel, 2016; Shaver et al., 2016) likely provide further evidence for the link between lung injury, inflammation, and hemoglobin fluctuations. These studies may offer insights into the specific mechanisms involved in this response.

3.7 Histological analysis

Rats without induced damage, Figures 6A, B, correspond to healthy lung tissue (control), demonstrating the normal histological architecture of the lung section. In damage rats with Chitosan Np (negative control) in Figures 6C, D, the lung tissue exhibited marked alveolar damage, underscored by disruption of the structural architecture. An increased inflammatory response with a significant macrophages

TABLE 1 Histopathological findings in lungs tissues rats exposed to Chitosan Np and Chitosan-IB (250 mg, 500 mg, 1000 mg) Np.

Lung tissue	Characteristic		
	Alveolar damage	Inflammation	Macrophage infiltration
Control			
Panel A and B	–	–	–
Negative control			
Panel C and D	++++	++++	+++
Damage + 250 mg			
Panel E and F	++	++	++
Damage + 500 mg			
Panel G and H	–	+	+
Damage +100 mg			
Panel I and J	++++	++++	++

Abbreviations: IB: ibuprofen; (–): no histopathological alterations; (+): histopathology in 10%–15% area; (++): histopathology in 20%–50% area; (+++): histopathology in 60%–70%; (++++): histopathology in >70% area.

infiltration, the white blood cells associated with inflammation and tissue repair, were observed. Severe tissue deformation emphasizes the severity of the damage and the severity of the lung injury over 72 h and provides the basis for a comparative evaluation of therapeutic interventions (Table 1).

In rats with damage and administration of the system of Chitosan-IB (250 mg) Np, resulted in a detectable reduction in inflammatory cell infiltration and tissue damage compared to negative control, as shown in Figures 6E, F. The inflammatory landscape was attenuated as shown by the reduced number of macrophages, indicating a dampened immune response. However, alveolar deformation persisted, albeit to a lesser extent, indicating that this dosage attenuated but did not completely halt the progression of damage, suggesting some efficacy of the drug at this dosage. Detailed analysis of Figures 6G, H shows that the system of Chitosan-IB (500 mg) Np represents a promising therapeutic scenario in which the alveoli retain their structural integrity. This finding is further supported by the presence of type II lipophages, cells naturally associated with lung tissue repair and regeneration processes, suggesting an active healing mechanism. The comparison with the control group and the group treated with Chitosan-IB (250 mg) Np suggests that the Chitosan-IB (500 mg) Np achieves an optimal balance in therapeutic efficacy, combining the prevention of damage with the activation of repair mechanisms, creating a favorable environment for healing. In addition, the reduction in macrophage presence underlines a significantly lower inflammatory response compared to the other groups, supporting the hypothesis that the Chitosan-IB (500 mg) Np may represent the most appropriate therapeutic window during the 72-h period studied and represents a significant improvement over previous option. Nevertheless, the escalated dose of 1,000 mg of the system Chitosan-IB (1,000 mg) Np (Figures 6I, J)again appears to lead to increased inflammation, with alveolar deformation and macrophage numbers mirroring those of untreated controls. This could indicate a possible overdose or saturation effect, where an excessive drug concentration either becomes ineffective or exacerbates condition. A summary of the results can be seen in Table 1. Considering the 72-h duration of action, it is obvious that the positive or negative effects of the drug manifest themselves relatively quickly. The observations between the different dosages underline the importance of dose optimization in therapeutic interventions. While the 500 mg dose seems promising, the unexpected results of the 1,000 mg dose show again that 'more' is not always 'better' when administering drugs.

The other organs of the different groups were also analyzed and showed no histological differences between them. The hearts showed no signs of inflammation or necrosis of the myocardium. The livers also showed no remarkable changes, apart from a lymphocytic infiltration in the periportal area. There was no tubular damage or necrosis in the kidneys, where toxicity is usually observed. The glomeruli also showed no changes.

4 Conclusion

In conclusion, this research successfully demonstrates the considerable potential of ibuprofen-loaded chitosan nanoparticles as a targeted therapeutic strategy for pulmonary conditions involving alveolar damage. The nanoparticles were efficiently synthesized and characterized, exhibiting high encapsulation efficiency, biocompatibility, and a dose-dependent effect on cell viability *in vitro*. Notably, *in vivo* experiments in a rat model of acute lung injury validated the therapeutic potential of these nanoparticles, with a 500 mg/mL dose over 72 h demonstrating optimal efficacy in reducing inflammation and promoting alveolar repair. These findings aid the way for further research to elucidate the underlying mechanisms of action and to validate these promising results in larger samples and over different time periods, ultimately

advancing the development of this innovative drug delivery system for targeted pulmonary therapy.

Data availability statement

The raw data supporting the conclusions of this article will be made available by the authors, without undue reservation.

Ethics statement

The animal study was approved by the Comité de Ética para la Investigación de la Facultad de Ingeniería de la Universidad Autónoma de Querétaro. The study was conducted in accordance with the local legislation and institutional requirements.

Author contributions

IO: Data curation, Formal Analysis, Investigation, Writing–original draft, Writing–review and editing. JM: Data curation, Formal Analysis, Writing–review and editing. VP: Conceptualization, Formal Analysis, Methodology, Supervision, Writing–review and editing. JC-G: Writing–review and editing, Data curation, Formal analysis, Validation, Software. MG: Data curation, Formal Analysis, Investigation, Methodology, Writing–review and editing. PG-S: Data curation, Formal Analysis, Visualization, Writing–review and editing. AÁ: Conceptualization, Data curation, Formal Analysis, Methodology, Writing–review and editing. VV: Data curation, Formal Analysis, Methodology, Visualization, Writing–review and editing. JR: Data curation, Formal Analysis, Methodology, Writing–review and editing. AR: Conceptualization, Data curation, Formal Analysis, Investigation, Methodology, Resources, Supervision, Validation, Visualization, Writing–original draft, Writing–review and editing. CG: Conceptualization, Data curation, Formal Analysis, Investigation, Methodology, Resources, Supervision, Validation, Visualization, Writing–original draft, Writing–review and editing.

Funding

The author(s) declare that financial support was received for the research, authorship, and/or publication of this article. CONVOCATORIA INVESTIGACION VINCULADA A LA ATENCION DE PROBLEMAS NACIONALES 2021 de la Facultad de Ingeniería, Universidad Autónoma de Querétaro (FIN 2021 11): Description: This fund provided the necessary financial resources to initiate the research project. Its role was fundamental in acquiring materials and laboratory equipment required to conduct the initial experiments and establish the project's foundation.

Acknowledgments

We would like to thank CONVOCATORIA INVESTIGACION VINCULADA A LA ATENCION DE PROBLEMAS NACIONALES 2021 from the Facultad de Ingeniería, Universidad Autónoma de Querétaro, with registration number FIN 2021 11, for funding this research. Additionally, we extend our gratitude to Instatext, which was used to check the grammar and spelling of the document. We also thank the Secretaría de Investigación, Innovación y Posgrado of the Universidad Autónoma de Querétaro for the financial support provided for the publication of this article.

Conflict of interest

The authors declare that the research was conducted in the absence of any commercial or financial relationships that could be construed as a potential conflict of interest.

Publisher's note

All claims expressed in this article are solely those of the authors and do not necessarily represent those of their affiliated organizations, or those of the publisher, the editors and the reviewers. Any product that may be evaluated in this article, or claim that may be made by its manufacturer, is not guaranteed or endorsed by the publisher.

References

Ambasch, G., Coscia, E., Luis, J., Díaz, T., Bueno, D., Argañarás, A., et al. (2021). Therapeutic potential of ibuprofen inhalation for COVID-19 pneumonia: report of two first cases. *J. Clin. Images Med. Case Rep.* 2. doi:10.52768/2766-7820/1336

Auvinen, J., Tapio, J., Karhunen, V., Kettunen, J., Serpi, R., Dimova, E. Y., et al. (2021). Systematic evaluation of the association between hemoglobin levels and metabolic profile implicates beneficial effects of hypoxia. *Sci. Adv.* 7 (29), eabi4822. doi:10.1126/sciadv.abi4822

Baek, J. S., Yeo, E. W., Lee, Y. H., Tan, N. S., and Loo, S. C. J. (2017). Controlled-release nanoencapsulating microcapsules to combat inflammatory diseases. *Drug Des. Dev. Ther.* 11, 1707–1717. doi:10.2147/DDDT.S133344

Calvo, P., Remuñan-López, C., Vila-Jato, J. L., and Alonso, M. J. (1997). Chitosan and chitosan/ethylene oxide-propylene oxide block copolymer nanoparticles as novel carriers for proteins and vaccines. *Pharm. Res.* 14 (10), 1431–1436. doi:10.1023/A:1012128907225

Chatterjee, S., and Hui, P. C. L. (2019). Review of stimuli-responsive polymers in drug delivery and textile application. *Molecules* 24 (14), 2547. doi:10.3390/MOLECULES24142547

CyQUANT MTT Cell Proliferation Assay Kit Protocol (2024). *Thermo Fisher scientific - MX*. Available at: https://www.thermofisher.com/mx/es/home/references/protocols/cell-and-tissue-analysis/protocols/vybrant-mtt-cell-proliferation-assay-protocol.html (Accessed July 8, 2024).

Fairbanks, V. F., Ziesmer, S. C., and O'Brien, P. C. (1992). Methods for measuring plasma hemoglobin in micromolar concentration compared. *Clin. Chem.* 38 (1), 132–140. doi:10.1093/CLINCHEM/38.1.132

Gaggar, A., and Patel, R. P. (2016). There is blood in the water: hemolysis, hemoglobin, and heme in acute lung injury. *Am. J. Physiology - Lung Cell. Mol. Physiology* 311 (4), L714–L718. doi:10.1152/ajplung.00312.2016

Gliszczyńska, A., and Sánchez-López, E. (2021). Dexibuprofen therapeutic advances: prodrugs and nanotechnological formulations. *Pharmaceutics* 13 (3), 414. doi:10.3390/PHARMACEUTICS13030414

Gulati, N., Dua, K., and Dureja, H. (2021). Role of chitosan based nanomedicines in the treatment of chronic respiratory diseases. *Int. J. Biol. Macromol.* 185, 20–30. doi:10.1016/J.IJBIOMAC.2021.06.035

Ha, M. W., and Paek, S. M. (2021). Recent advances in the synthesis of ibuprofen and naproxen. *Mol. Basel, Switz.* 26 (16), 4792. doi:10.3390/MOLECULES26164792

Hassani, S., Laouini, A., Fessi, H., and Charcosset, C. (2015). Preparation of chitosan–TPP nanoparticles using microengineered membranes – effect of parameters and encapsulation of tacrine. *Colloids Surfaces A Physicochem. Eng. Aspects* 482, 34–43. doi:10.1016/J.COLSURFA.2015.04.006

He, S., Gui, J., Xiong, K., Chen, M., Gao, H., and Fu, Y. (2022). A roadmap to pulmonary delivery strategies for the treatment of infectious lung diseases. *J. Nanobiotechnology* 20 (1), 101–122. doi:10.1186/S12951-022-01307-X

Huang, G., Liu, Y., and Chen, L. (2017). Chitosan and its derivatives as vehicles for drug delivery. *Drug Deliv.* 24 (2), 108–113. doi:10.1080/10717544.2017.1399305

Kim, Y., Zharkinbekov, Z., Kamila, R., Laura, T., Kamila, B., Dias, Z., et al. (2023). Chitosan-based biomaterials for tissue regeneration. *Pharmaceutics* 15 (3), 807. doi:10.3390/pharmaceutics15030807

Liu, H., Wang, C., Li, C., Qin, Y., Wang, Z., Yang, F., et al. (2018). A functional chitosan-based hydrogel as a wound dressing and drug delivery system in the treatment of wound healing. *RSC Adv.* 8 (14), 7533–7549. doi:10.1039/C7RA13510F

Mansour, A., Romani, M., Acharya, A. B., Rahman, B., Verron, E., and Badran, Z. (2023). Drug delivery systems in regenerative medicine: an updated review. *Pharmaceutics* 15 (2), 695. doi:10.3390/PHARMACEUTICS15020695

McGee, J. S., Meraz, R., Myers, D. R., and Davie, M. R. (2020). Telehealth services for persons with chronic lower respiratory disease and their informal caregivers in the context of the COVID-19 pandemic. *Pract. Innov.* 5 (2), 165–177. doi:10.1037/PRI0000122

Newman, S. P. (2017). Drug delivery to the lungs: challenges and opportunities. *Ther. Deliv.* 8 (8), 647–661. doi:10.4155/TDE-2017-0037

Party, P., Klement, M. L., Szabó-Révész, P., and Ambrus, R. (2023). Preparation and characterization of ibuprofen containing nano-embedded-microparticles for pulmonary delivery. *Pharmaceutics* 15 (2), 545. doi:10.3390/pharmaceutics15020545

Patrisio, N. N. (2020). Host-microbe-drug triad: role of chloroquine/hydroxychloroquine in Covid-19 treatment-focus on inflammatory cytokine inhibition. *Afr. J. Microbiol. Res.* 14 (12), 644–647. doi:10.5897/AJMR2020.9403

Pontes, J. F., and Grenha, A. (2020). Multifunctional nanocarriers for lung drug delivery. *Nanomaterials* 10 (2), 183. doi:10.3390/NANO10020183

Rosa, C. M., Mereles, S. M., Rigacci, M. F., and Colimodio, D. C. (2020). Hemoglobina libre en plasma por espectrofotometría directa. *Rev. Hematol.* 24 (2), 91–96.

Saha, P., Chowdhury, S., Gupta, S., Kumar, I., and Kumar, R. (2010). Assessment on the removal of malachite green using tamarind fruit shell as biosorbent. *Clean. – Soil, Air, Water* 38 (5–6), 437–445. doi:10.1002/CLEN.200900234

Shaver, C. M., Upchurch, C. P., Janz, D. R., Grove, B. S., Putz, N. D., Wickersham, N. E., et al. (2016). Cell-free hemoglobin: a novel mediator of acute lung injury. *Am. J. Physiology - Lung Cell. Mol. Physiology* 310 (6), L532–L541. doi:10.1152/ajplung.00155.2015

Türkmen, E. U., Arslan, P., Erkoç, F., Günal, A. Ç., and Duran, H. (2024). The cerium oxide nanoparticles toxicity induced physiological, histological and biochemical alterations in freshwater mussels, Unio crassus. *J. Trace Elem. Med. Biol.* 83, 127371. doi:10.1016/J.JTEMB.2023.127371

Xu, Y., Dong, X., Xu, H., Jiao, P., Zhao, L.-X., and Su, G. (2023). Nanomaterial-based drug delivery systems for pain treatment and relief: from the delivery of a single drug to Co-delivery of multiple therapeutics. *Pharmaceutics* 15 (9), 2309. doi:10.3390/PHARMACEUTICS15092309

Yang, B., Dong, Y., Wang, F., and Zhang, Y. (2020). Nanoformulations to enhance the bioavailability and physiological functions of polyphenols. *Molecules* 25 (20), 4613. doi:10.3390/MOLECULES25204613